

## Supporting Information

### **Biochar carbon stability in a clayey soil as a function of feedstock and pyrolysis temperature**

Bhupinder Pal Singh<sup>1,2\*</sup>, Annette L Cowie<sup>1,2</sup>, Ronald J Smernik<sup>3</sup>

<sup>1</sup>NSW Department of Primary Industries, PO Box 100, Beecroft NSW 2119, Australia

<sup>2</sup>Rural Climate Solutions, University of New England, Armidale 2351, Australia

<sup>3</sup>School of Agriculture, Food & Wine and Waite Research Institute, The University of Adelaide, Waite Campus, Urrbrae, South Australia 5064, Australia

\*Corresponding author. Bhupinder Pal Singh ([bp.singh@dpi.nsw.gov.au](mailto:bp.singh@dpi.nsw.gov.au))

**Number of pages** = S23

**Number of figures** = S8

**Number of tables** = S3

**Soils and Biochars.** The landscape in the area of soil sampling has been dominated by the largely treeless plains of Mitchell grass for over 100 years (David Phelps Pers. Comm.). Clay minerals were identified by X-ray diffraction analysis of basally oriented specimens<sup>1</sup>.

The biochars were produced using slow pyrolysis (Daisy Reactor, Pacific Pyrolysis, Australia) at a heating rate of 5–10 °C/min, with 40 min residence time in the reactor at the highest heating temperature (HTT). Nitrogen (N<sub>2</sub>) gas was then added into the reactor during the cooling-off period to maintain an inert environment<sup>3</sup>. The activation treatment involved introduction of steam for the entire 40 min residence time in the reactor at the HHT. This activation process leads to the development of a highly porous biochar structure<sup>2</sup>.

The finely ground (<53 µm) soil and biochar samples were analysed for  $\delta^{13}\text{C}$  by isotope ratio mass spectrometry (IRMS). We used a Micromass IsoPrime IRMS with analytical precision ( $1\sigma$ ) < 0.10–0.15‰ (determined from acetanilide standard) or a Delta V Thermo Finnigan IRMS with analytical precision ( $1\sigma$ ) < 0.10‰ (determined from beet sucrose standards)<sup>1</sup>.

Repeated acid-washing of biochar samples was performed<sup>3</sup> to determine if biochars contained  $^{13}\text{C}$ -enriched carbonates. The  $\delta^{13}\text{C}$  values of biochars (except for PS550A) did not change after repeated acid washing. The  $\delta^{13}\text{C}$  value of PS550A became more negative (from -21.7‰ to -26.2‰), likely due to the loss of  $^{13}\text{C}$ -enriched carbonates in the PS550A biochar during acid washing.

The enrichment of  $\delta^{13}\text{C}$  of PS550A (*cf.* parent feedstock) is likely due to an increased concentration of calcite following pyrolysis, because the temperature for thermal degradation of calcite is higher than the pyrolysis temperature used in our study<sup>3</sup>.

**$^{13}\text{C}$  NMR Analyses of Biochars.** Biochar samples were packed in 7-mm diameter cylindrical zirconia rotors with Kel-F rotor end-caps and spun at the “magic angle” ( $54.7^\circ$ ) at  $6500 \pm 100$  Hz in a Doty Scientific supersonic MAS probe. Free induction decays were acquired with a sweep width of 50 kHz; 1216 data points were collected over an acquisition time of 12 ms. All spectra were zero-filled to 8192 data points and processed with a 50-Hz Lorentzian line broadening and a 0.010-s Gaussian broadening. Chemical shifts were externally referenced to the methyl resonance of hexamethylbenzene at 17.36 ppm. Cross polarization spectra represent the accumulation of 4000 scans and were acquired using a  $90^\circ$   $^1\text{H}$  pulse of 5-6  $\mu\text{s}$  duration, a 1-ms contact time and a 1-s recycle delay. Direct polarization spectra represent the accumulation of 500-1000 scans and were acquired using a  $90^\circ$   $^{13}\text{C}$  pulse of 5-10  $\mu\text{s}$  duration and a 90-s recycle delay.

Signal due to non-aromatic alkyl and O-alkyl C was quantified using a deconvolution procedure<sup>4</sup>, in which the spectra were simulated as the sum of Lorentzian-shaped peaks. Nine peaks were used for fits to the spectra of the 400 °C biochars (aromatic peak + 4 SSBs, O-aryl, O-alkyl and  $2 \times$  alkyl), whereas seven peaks were used for fits to the spectra of the 550 °C biochars (aromatic peak + 4 SSBs, O-aryl, and alkyl).

Spin counting was carried out using the method of Smernik and Oades<sup>5</sup> to determine the strength of the NMR signal of the sample i.e. calibrated against a quantitative

signal of a reference material (glycine; AR grade, Ajax Chemicals). Spin counting showed that the C observability by CP ( $C_{\text{obs}} \text{ CP}$ )  $^{13}\text{C}$  NMR was in the range 18–43%, with the lowest values (18–23%) for the biochars with the lowest C content, i.e. those produced from paper sludge and cow manure (Table S1). This suggests that paramagnetic or ferromagnetic minerals in these biochars may have interfered with NMR detection. Values of  $C_{\text{obs}} \text{ (DP)}$  were in the range 57–79%, with the lowest value being for the biochar produced from paper sludge. On average,  $C_{\text{obs}} \text{ (DP)}$  was 2.3 times greater than  $C_{\text{obs}} \text{ (CP)}$ . The most likely cause of under-detection of signal in DP spectra is that the time between scans (90 s), known as the recycle delay, was insufficient to enable complete relaxation.

**Incubation Experiment.** A microbial inoculum was prepared by mixing soil samples collected from native eucalyptus forests, pine plantation, maize cropping and grazed pastures, to introduce a diverse range of microbial communities to the incubated soil<sup>1</sup>. Each soil jar was inoculated with ~1 g of microbial inoculum. “Blank” buckets, containing empty sealed containers, were also included along with biochar treatments for each replicate to account for  $\text{CO}_2\text{-C}$  and associated  $\delta^{13}\text{C}$  of the bucket atmosphere. The soil was maintained at ~70% water holding capacity (~23% moisture content (w/w)) throughout by periodically adjusting any moisture loss during incubation. The three replicates were staggered in time (i.e. commenced at one week intervals). In total, 87 buckets across 12 treatments (including 3 blank buckets) were set up for each of the three replicates to allow removal of biochar-soil mixtures at 0 days, 9 days, 63 days, 196 days, 1 year, 2 years, and 4 years after incubation. A new  $\text{CO}_2$  trap (2 M NaOH) was introduced at 3, 9, 20, 42, 63, 84, 133, 196, 287, 364, 462, 581, 728, 847,

966, 1064, 1274, 1450, 1660 and 1829 days. The CO<sub>2</sub> traps from 3 buckets for each treatment were analysed for total CO<sub>2</sub>-C and  $\delta^{13}\text{C}$ .

**Carbon Mineralization and Mean Residence Time of Biochars.** The CO<sub>2</sub> absorbed in 1 mL of 2 M NaOH was precipitated with 10 mL of 0.25 M BaCl<sub>2</sub> and the residual NaOH was titrated with 0.1 M HCl using phenolphthalein as the indicator<sup>6</sup>. To another 10 mL aliquot of 2 M NaOH, 10 mL of 1 M SrCl<sub>2</sub>·6H<sub>2</sub>O was added to precipitate the trapped CO<sub>2</sub> as SrCO<sub>3</sub>. The SrCO<sub>3</sub> precipitate was repeatedly washed (~8 times) with deionised water to obtain a neutral pH in the supernatant. The supernatant was discarded and the precipitate was dried at 60 °C and finely-ground for  $\delta^{13}\text{C}$  analysis by IRMS (1.5 mg SrCO<sub>3</sub> + 3 mg V<sub>2</sub>O<sub>5</sub> using a Delta V Thermo Finnigan IRMS or 4 mg SrCO<sub>3</sub> + 6 mg V<sub>2</sub>O<sub>5</sub> using a Micromass IsoPrime IRMS)<sup>7</sup>.

In the isotope mixing model (see Equation 1 in the main paper), the  $\delta^{13}\text{C}$  value of soil CO<sub>2</sub>-C, as a fraction of total CO<sub>2</sub>-C evolved from the biochar-amended soils, was assumed to be similar to the control soil.

In the case of biochar, we used the initial  $\delta^{13}\text{C}$  signature of biochar C in the isotope mixing model. It is possible that the labile C compounds in biochars have different  $\delta^{13}\text{C}$  signatures than the  $\delta^{13}\text{C}$  signature of whole biochar C. However, this seems unlikely as we only recorded a small change (for wood) or no change (for leaf and manures) in the  $\delta^{13}\text{C}$  signature between the parent feedstocks and corresponding biochars following pyrolysis, relative to the large differences between the  $\delta^{13}\text{C}$  signatures of the C3 biochars and C4 soil organic matter (see Materials and Methods and Table 1 in the main manuscript). Furthermore, the  $\delta^{13}\text{C}$  signature of the light C

fraction (density  $\sim 1.85 \text{ g cm}^{-3}$ ), which recovered *ca.* 93-95% of wood, leaf and poultry litter biochar C, and *ca.* 68-75% of cow manure biochar C, were not significantly different on day 0, and after 1 year and 2 years of incubation (data not shown). These data suggest that the  $\delta^{13}\text{C}$  signatures of decomposed (relatively labile) and remaining (relatively stable) components of biochars remained similar and any  $^{13}\text{C}$  fractionation during biochar C mineralization was minimal. Finally, the repeated acid-washing treatment<sup>3</sup>, which could also remove some soluble organic C, did not result in significant changes in the  $\delta^{13}\text{C}$  values of biochars after acid washing (data not shown). These results provided further evidence for the homogeneity of  $\delta^{13}\text{C}$  values across the C components of biochar and hence supporting the use of the initial  $\delta^{13}\text{C}$  value of biochar in the isotope mixing model (Equation 1 in the main paper).

The cumulative amount of organic C in biochar-amended and control soils was calculated by multiplying the daily rate of organic C mineralization at each sampling time by the number of days between measurements, and subsequent stepwise addition of the total organic C mineralized over the duration of incubation.

The cumulative % of biochar or native soil organic C mineralized was calculated as the cumulative amount ( $\text{mg kg}^{-1}$  soil) of  $\text{CO}_2\text{-C}$  evolved at different times over 5 years expressed as a percentage of the initial amount ( $\text{mg kg}^{-1}$  soil) of biochar C or native soil organic C, respectively.

The cumulative amounts of biochar C mineralized over 5 years varied between 101 and  $244 \text{ mg kg}^{-1}$  soil for the  $400^\circ\text{C}$  biochars, and between 30 and  $73 \text{ mg kg}^{-1}$  soil for the  $550^\circ\text{C}$  biochars, excluding the PS550A biochar (Figure S6). The differences

between the additional (i.e. amended minus non-amended) soil C mineralized (Figure S4c–d) and biochar C mineralized (Figure S6a–b) over 5 years ranged between 31 and 156 mg kg<sup>-1</sup> soil for the 400 °C biochars, and between -3.5 and 38 mg kg<sup>-1</sup> soil for the 550 °C biochar treatments; these values represent the overall primed soil organic C mineralized in the presence of biochars (Figure S8a, b). Although the overall loss of native soil C due to priming effect of biochar is positive for most biochar treatments, we observed a constant stabilisation of native soil organic C from 2.5 years onward (data not shown). The detailed data on the dynamics of biochar induced primed soil C over 5 years will be published separately.

The course of the cumulative % of biochar C or native C mineralized during experimental periods was fitted to a two pool exponential model<sup>1</sup>. The equation for the model is given below:

$$C_{Bt}(\%) = C_L(1 - e^{-k_L t}) + (100 - C_L)(1 - e^{-k_R t})$$

where  $C_{Bt}(\%)$  is the cumulative % of biochar-C mineralized;  $C_L$  and  $(100 - C_L)$  are the proportions the labile (easily-mineralizable) and recalcitrant (slowly-mineralizable) pools in biochar-C, respectively;  $k_L$  and  $k_R$  are the mineralization rate constants for the labile and recalcitrant pools, respectively; and  $t$  is the incubation time (days). The Solver add-in tool in Microsoft Excel was used to estimate the values of the model parameters by minimizing the sum of the squared errors between modelled and measured values of the % cumulative biochar-C mineralized at different times over 5 years. The mean residence time (MRT) is the inverse ( $1/k_L$  or  $1/k_R$ ) of the mineralization rate constant.

**Statistical Analyses.** To allow for correlation between repeated measures on the same units, a first order or second order autoregressive model was fitted (giving a higher residual log-likelihood than the power model). Heterogeneity in the residual variances between time-points was included as it was significant using a residual likelihood ratio test. Wald-type F statistics (with Kenward-Roger adjustments) were calculated for all fixed terms.



## References

1. Keith, A.; Singh, B.; Singh, B. P. Interactive priming of biochar and labile organic matter mineralization in a smectite-rich soil. *Environ. Sci. Technol.* **2011**, *45* (22), 9611–9618.
2. Downie, A., Crosky, A. & Munroe, P. Physical properties of biochar. In: *Biochar for environmental management: Science and technology*, (Eds. Lehmann, J. & Joseph, S.), Earthscan, London (2009).
3. Singh, B.; Singh, B. P.; Cowie, A. L. Characterisation and evaluation of biochars for their application as a soil amendment. *Aust. J. Soil Res.* **2010**, *48*, 516–525.
4. McBeath, A. V.; Smernik, R. J.; Schneider, M. P.; Schmidt, M. W.; Plant, E. L. Determination of the aromaticity and the degree of aromatic condensation of a thermosequence of wood charcoal using NMR. *Org. Geochem.* **2011**, *42*, 1194–1202.
5. Smernik, R. J.; Oades, J. M. The use of spin counting for determining quantitation in solid state <sup>13</sup>C NMR spectra of natural organic matter 2. HF-treated soil fractions. *Geoderma* **2000**, *96*, 159–171.
6. Bhupinderpal-Singh.; Rengel, Z.; Bowden, J. W. Carbon, nitrogen and sulphur cycling following incorporation of canola residue of different sizes into a nutrient-poor sandy soil. *Soil Biol. Biochem.* **2006**, *38*, 32–42.
7. Harris, D.; Porter, L. K.; Paul, E. A. Continuous flow isotope ratio mass spectrometry of carbon dioxide trapped as strontium carbonate. *Commun. Soil Sci. Plan. Anal.* **1997**, *28*, 747–757.

**Table S1. Results of spin counting on solid-state  $^{13}\text{C}$  CP and DP NMR spectra.**

Sample	C <sub>obs</sub> (CP) (%)	C <sub>obs</sub> (DP) (%)
Wood 400°C, activated	26	68
Wood 550°C, activated	28	73
Wood 400°C, non-activated	30	77
Wood 550°C, non-activated	36	73
Leaves 400°C, activated	35	72
Leaves 550°C, activated	28	79
Paper sludge 550°C, activated	23	57
Poultry litter 400°C, non-activated	43	73
Poultry litter 550°C, activated	31	66
Cow manure 400°C, non-activated	23	
Cow manure 550°C, activated	18	

**Table S2. Mean residence time (MRT) of biochar carbon in soil (vertisol), estimated by fitting the two-pool model to the cumulative biochar C mineralization data at different times over 5 years.**

Treatments	Mean residence time (years) at different times of incubation					
	196 d	364 d	728 d	1064 d	1450 d	1829 d
<b>400 °C biochars</b>						
Wood400A	217	231	299	375	341	326
Wood400NA	208	219	278	321	302	294
Leaf400A	136	171	220	275	274	270
PL400NA	51	73	103	126	127	129
CM400NA	47	65	87	101	95	90
<b>550 °C biochars</b>						
Wood550A	1054	1267	1337	1491	1371	1271
Wood550NA	952	1374	1982	1968	1758	1616
Leaf550A	353	518	706	796	638	572
PS550A	370	452	512	518	437	396
PL550A	151	202	299	386	331	313
CM550A	1054	1267	1337	1491	1371	1271

**Table S3. The predictive relationships of biochar stability parameters (mean residence time and cumulative % of added biochar carbon mineralized) with the  $^{13}\text{C}$  CP NMR-derived properties of biochar C (aromatic condensation and % non-aromatic carbon) at different times over 5 years of incubation. The associated variation explained by the fitted models and the significance of the relationships are also shown.**

Time of incubation	x = aromatic condensation ( $-\Delta\delta$ )	Adjusted $R^2$ (%)	$P$	x = % non-aromatic C	Adjusted $R^2$ (%)	$P$
<b>y = Mean residence time</b>						
196	$y = 93.4e^{1.184x}$	92.6	<0.001	$y = 1165x^{-0.717}$	92.3	<0.001
364	$y = 113.6e^{1.226x}$	93.7	<0.001	$y = 1553x^{-0.744}$	93.9	<0.001
728	$y = 148.0e^{1.216x}$	89.6	<0.001	$y = 1967x^{-0.742}$	89.6	<0.001
1064	$y = 181.7e^{1.130x}$	92.6	<0.001	$y = 2021x^{-0.688}$	91.9	<0.001
1450	$y = 156.4e^{1.153x}$	94.7	<0.001	$y = 1828x^{-0.704}$	93.6	<0.001
1829	$y = 148.0e^{1.140x}$	95.3	<0.001	$y = 1682x^{-0.696}$	94.0	<0.001
<b>y = Biochar carbon mineralized (% of total)</b>						
196	$y = 0.55x^{-0.864}$	59.5	0.002	$y = 0.19e^{0.097x}$	70.1	<0.001
364	$y = 0.65x^{-0.858}$	65.8	<0.001	$y = 0.24e^{0.094x}$	76.3	<0.001
728	$y = 0.81x^{-0.857}$	72.8	<0.001	$y = 0.31e^{0.092x}$	82.7	<0.001
1064	$y = 0.95x^{-0.852}$	77.0	<0.001	$y = 0.39e^{0.090x}$	85.6	<0.001
1450	$y = 1.21x^{-0.849}$	83.2	<0.001	$y = 0.52e^{0.087x}$	89.4	<0.001
1829	$y = 1.43x^{-0.843}$	86.4	<0.001	$y = 0.64e^{0.085x}$	90.9	<0.001

## Figure captions

### **Figure S1. Solid-state $^{13}\text{C}$ CP NMR spectra of the eleven biochars.**

The spectra are the accumulation of 4000 scans, representing an acquisition time of approximately 2.5 hours. All spectra are dominated by the aromatic resonance at approximately 130 ppm and associated spinning sidebands (SSBs), which are artifacts that appear approximately 65 ppm and 130 ppm either side of the central aromatic band (i.e. at approximately 230 ppm, 195 ppm, 65 ppm and 0 ppm). A shoulder is apparent on the left side of the main aromatic peak for most of the 400 °C biochars. This can be attributed to O-substituted aromatic carbon. The spectra of the biochars produced from eucalyptus wood and leaves at 400 °C contain a small, sharp peak at approximately 165 ppm. This is consistent with either oxylate or bicarbonate carbon. Clear signals due to alkyl C appear in the 10-40 ppm region of the 400 °C biochars. Much smaller alkyl C signals can be discerned in the same region of the 550 °C biochars, where they appear as a shoulder on the left side of the aromatic SSB at approximately 0 ppm. Small signals due to O-substituted alkyl C (O-alkyl C) appear as a shoulder on the left side of the aromatic SSB at approximately 65 ppm only for the 400 °C biochars.

### **Figure S2. Solid-state $^{13}\text{C}$ DP NMR spectra of nine of the eleven biochars. DP spectra of adequate quality could not be obtained for the biochars produced from cow manure.**

The DP spectra are generally very similar in appearance to the corresponding CP spectra (Fig. 1S), although signals for non-aromatic signal are slightly less intense relative to the aromatic signal. One major difference between CP and DP spectra is

apparent for the biochar produced from paper sludge at 550 °C, the DP spectrum of which contains a strong, sharp resonance at 166 ppm that is completely absent in the corresponding CP spectrum. This can be attributed to carbonate, which is not detected by CP due to the lack of H atoms in the carbonate structure. No attempt was made to quantify the non-aromatic C signal in the DP spectra because the poorer signal-to-noise ratios adversely affect the reliability of the fitting procedure. However, given the similarity of the CP and DP spectra, but the slightly lower signal intensities for non-aromatic signals in the DP spectra, it can be assumed that the percentages of non-aromatic signal determined from the CP spectra (see Table 1 in the main paper) are a slight over-estimation of the percentages of non-aromatic C in the biochars.

**Figure S3. Relationship between the  $^{13}\text{C}$  CP NMR derived properties of biochar carbon i.e. degree of aromatic condensation and proportion of non-aromatic C (% of total signal).**

**Figure S4. Total carbon (C) mineralization rate ( $\text{mg CO}_2\text{-C kg}^{-1}\text{ soil d}^{-1}$ ; upper panel) and cumulative amount of soil carbon mineralized ( $\text{mg CO}_2\text{-C kg}^{-1}\text{ soil}$ ; lower panel) during 5 years incubation in the presence of low temperature (400 °C; Fig. a, c) and high temperature (550 °C; Fig. b, d) biochars in a smectite-rich vertisol.** Treatment details are given in the main paper (see the Materials and Method section). The insets in Fig. a, b show the total C mineralization rate from 66 days after incubation with an expanded y-axis scale for clarity. Note the change of scale after the break on the x-axis (i.e. duration of incubation). Error bars (Fig. c, d) represent  $\pm$  standard error of the mean ( $n = 3$ ). Blue bars in (Fig. a, b, including in insets) show least significant differences (at 5% level,  $\text{LSD}_{0.05}$ ).

**Figure S5. Cumulative % of total carbon (C) mineralized during 5 years incubation in the presence of low temperature (400 °C; Fig. a) and high temperature (550 °C; Fig. b) biochars in a smectite-rich vertisol.** Treatment details are given in the Materials and Methods in the main paper. Note the change of scale after the break on the x-axis (i.e. duration of incubation). Error bars represent  $\pm$  standard error of the mean ( $n = 3$ ).

**Figure S6. Percentage of biochar-derived carbon (C) in total (soil plus biochar) C mineralized (upper panel) and  $\delta^{13}\text{C}$  values of total carbon released (lower panel) from 400 °C (Fig. a, c) and 550 °C (Fig. b, d) biochar-amended or control soils at different times during 5 years incubation.** Treatment details are given in the Materials and Methods. Note the change of scale after the break on the x-axis (i.e. duration of incubation). Error bars represent  $\pm$  standard error of the mean ( $n = 3$ ).

**Figure S7. Cumulative amount of biochar carbon (C) mineralized ( $\text{mg CO}_2\text{-C kg}^{-1}$  soil) during 5 years' incubation in the presence of low temperature (400 °C; left panel) and high temperature (550 °C; right panel) biochars in a smectite-rich vertisol.** Treatment details are given in the Materials and Methods. Note the change of scale after the break on the x-axis (i.e. duration of incubation). Error bars represent  $\pm$  standard error of the mean ( $n = 3$ ).

**Figure S8. Budget of cumulative carbon (C) mineralized over 5 years from biochar and native organic matter sources, including the native C mineralized due to the priming effect, from vertisol amended with 400 °C (left panel) and 550 °C (right panel) biochars.** Treatment details are given in the Materials and Methods.

Figure S1

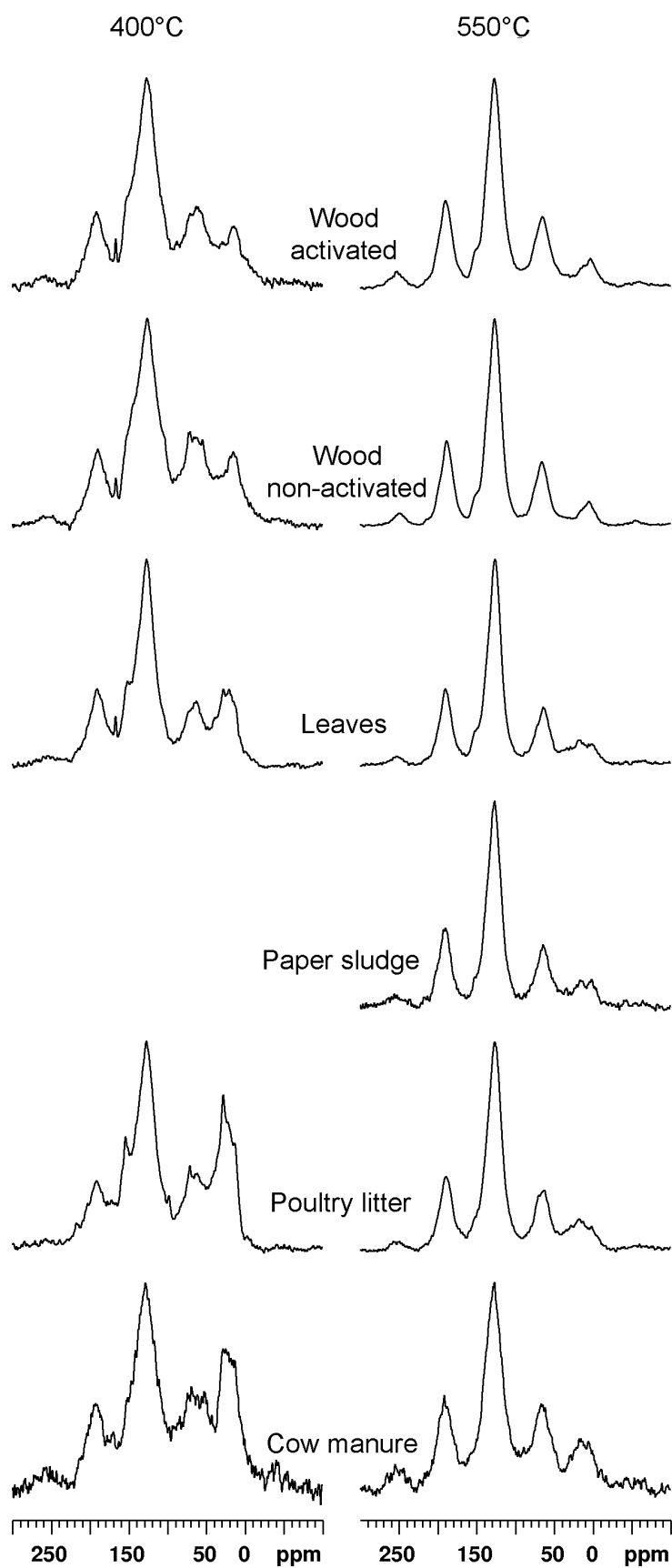




Figure S2

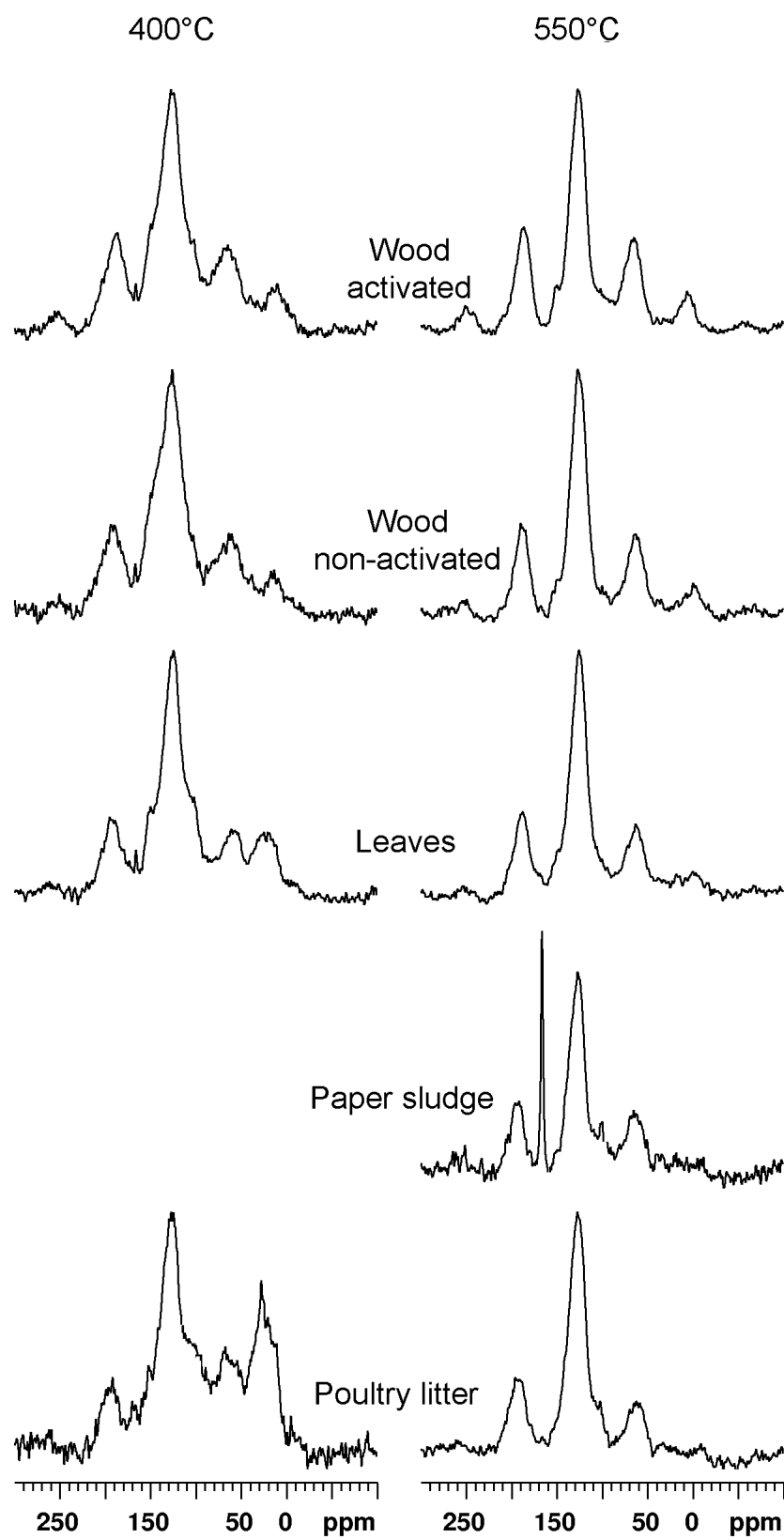


Figure S3

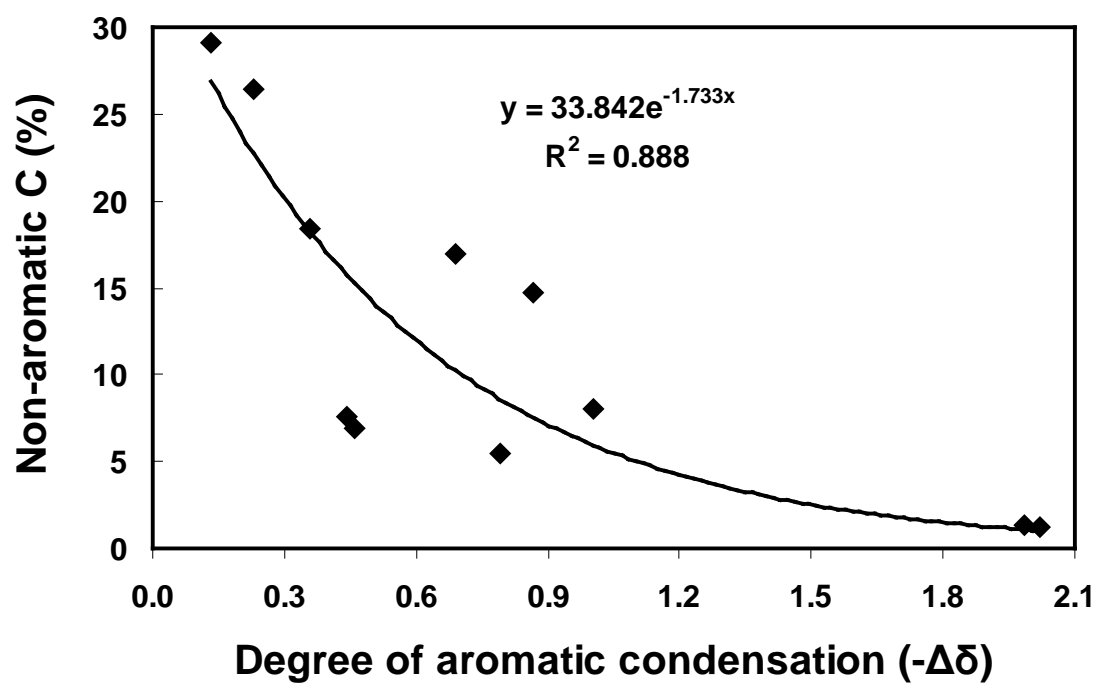


Figure S4

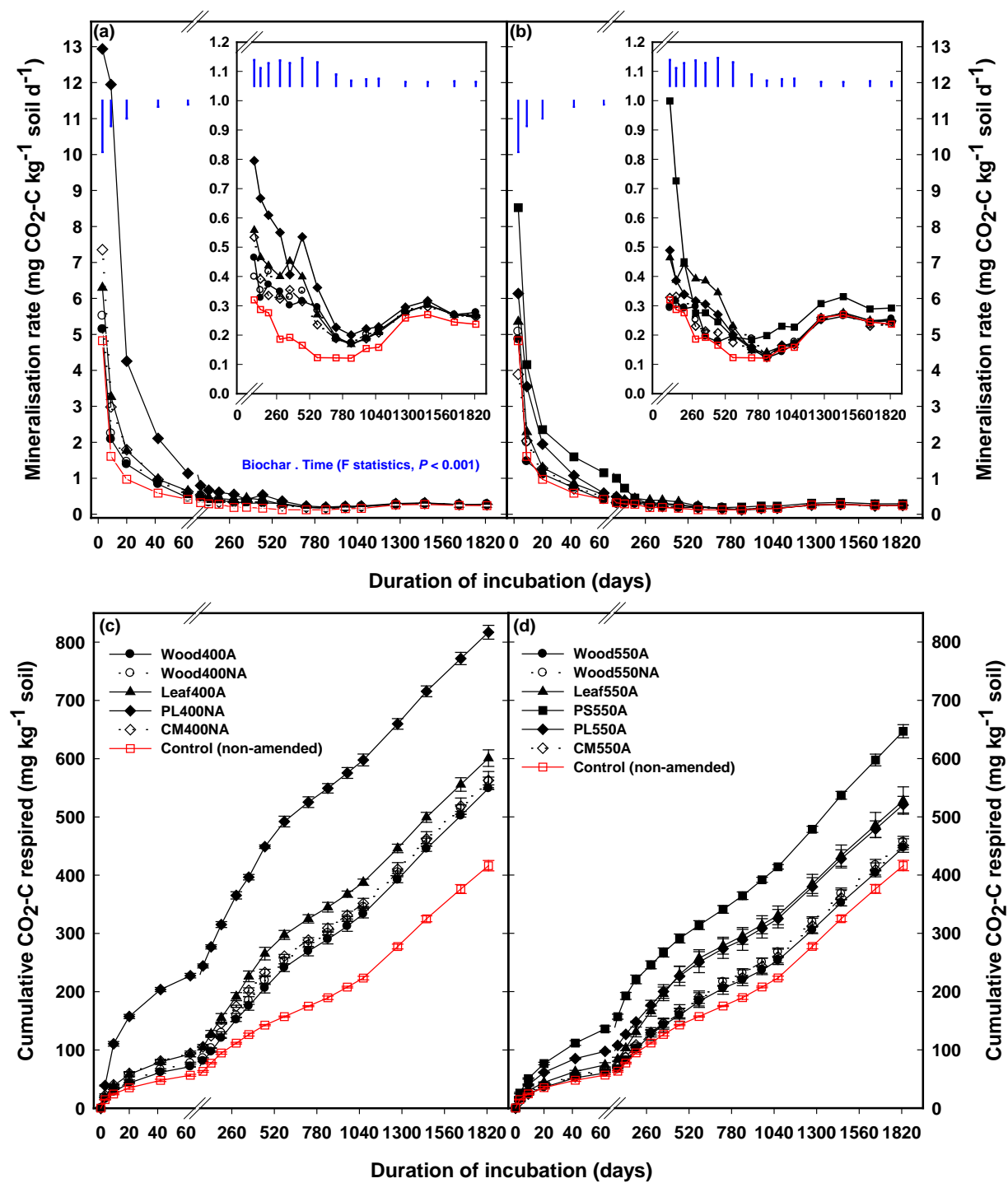


Figure S5

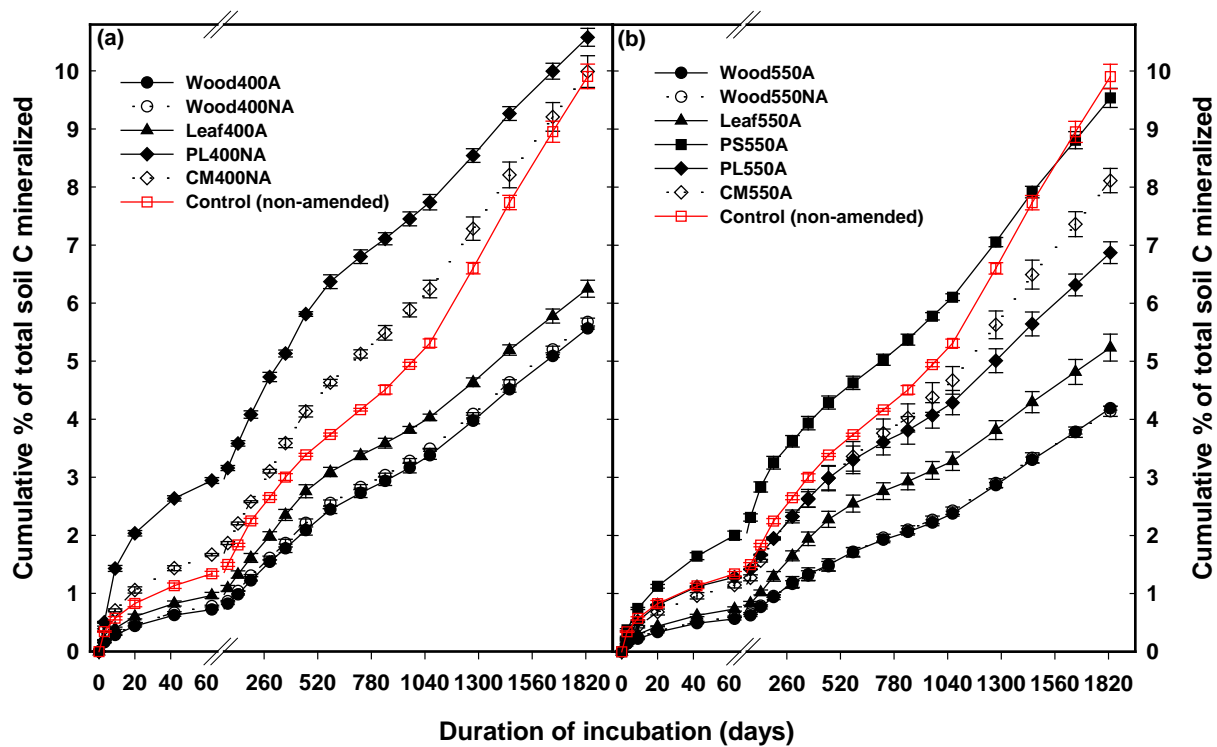


Figure S6

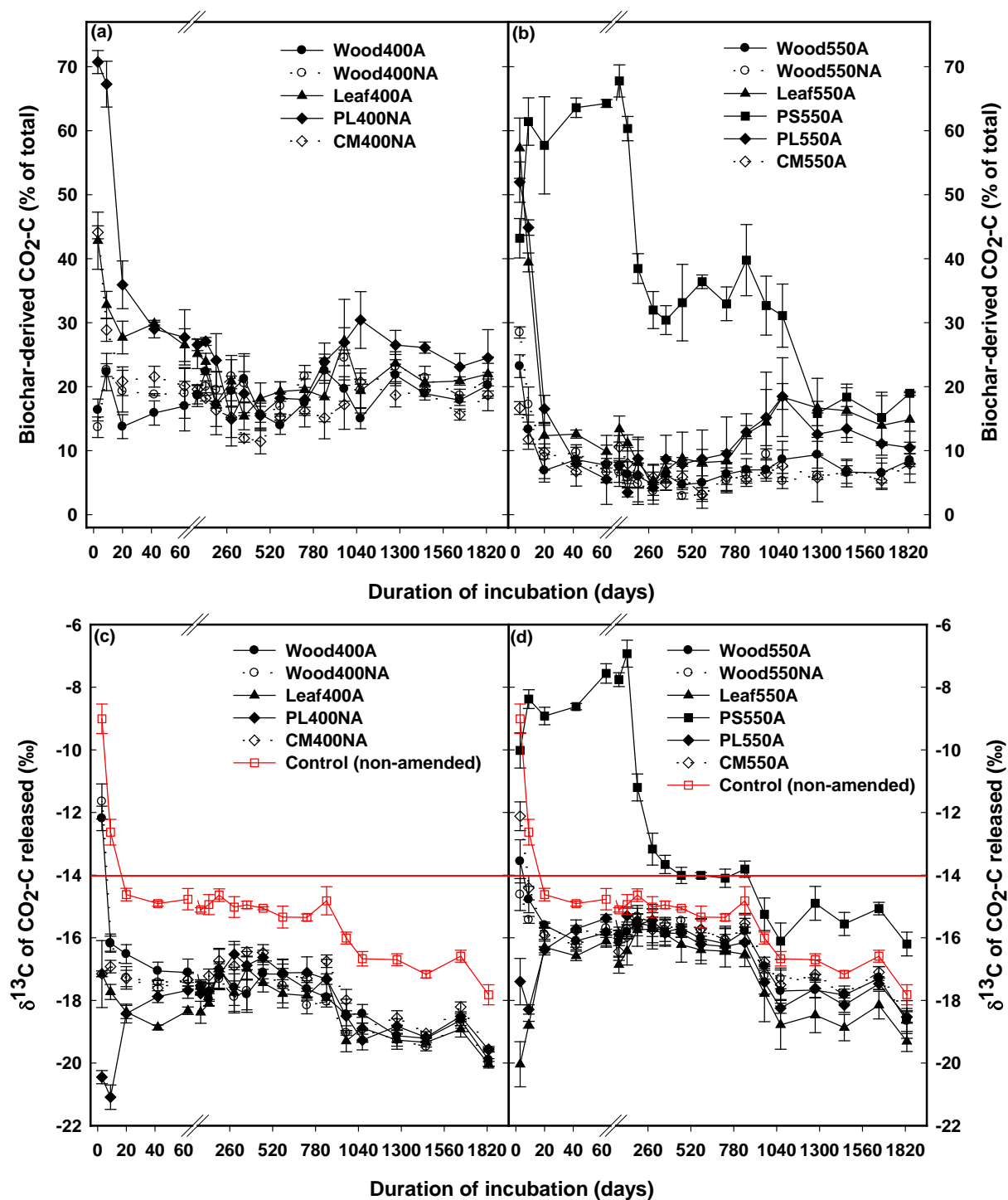




Figure S8

